Nanoscale

COMMUNICATION

In situ chemoresistive sensing in the environmental TEM: probing functional devices and their nanoscale morphology

Received 00th January 20xx,
Accepted 00th January 20xx

DOI: 10.1039/x0xx00000x

www.rsc.org/

Stephan Steinhauer,[a] Jerome Vernieres,[a] Johanna Krainer,[b] Anton Köck,[b] Panagiotis Grammatikopoulos[a] and Mukhles Sowwan*[a]

***In situ* transmission electron microscopy (TEM) provides exciting opportunities in order to address fundamental questions and technological aspects related to functional nanomaterials, including the structure-property relationships of miniaturized electronic devices. Herein, we report *in situ* chemoresistive sensing in the environmental TEM with a single SnO_2 nanowire device, studying the impact of surface functionalization with heterogeneous nanocatalysts. By detecting toxic carbon monoxide (CO) gas at ppm-level concentration inside the microscope column, the sensing properties of a single SnO_2 nanowire were characterized before and after decoration with hybrid Fe-Pd nanocubes. Structural changes of the supported nanoparticles induced by sensor operation were revealed, enabling the direct correlation with CO sensing properties. Our novel approach is applicable for a broad range of functional nanomaterials and paves the way for future studies on the relationship between chemoresistive properties and nanoscale morphology.**

Despite the continuous increase in demand for miniaturized, low-cost sensors based on chemoresistive nanostructures, the complex morphology dependence of sensing activity remains to a large extent unexplored, in particular for the widely used semiconducting metal oxide materials.[1] In order to optimize the performance of these sensor devices, surface functionalization with catalytic nanoparticles has been extensively investigated for improved selectivity[2-3] and low operation temperature;[4-6] however, only limited information is available on the interplay between the atomic-scale structure of the employed nanocatalysts and their impact on chemoresistive sensing properties. To address these shortcomings, we introduce a novel approach based on *in situ* probing of functional sensor devices by environmental transmission electron microscopy (TEM). Over the years, *in situ* TEM has become a powerful tool for studying chemical reactions in gas/liquid environments while applying elevated temperatures and/or electrical bias.[7] It has been utilized in diverse research areas ranging from materials to life sciences, offering unique capabilities for studies on various dynamic processes at the atomic scale, such as phase transitions,[8] oscillatory catalytic reactions,[9] mechanical deformation,[10] or catalytic[11] and non-catalytic[12] nanowire growth. Moreover, *in situ* experiments have been performed in order to establish structure-property relationships of functional devices, for instance in applications such as Li-ion batteries,[13-14] graphene field effect transistors[15] or resistive switching memory devices.[16-18]

Herein, we demonstrate chemoresistive sensing in the environmental TEM for *in situ* characterization of heterogeneous nanocatalysts deposited on the sensor surface. As an exemplary case, we study the detection of toxic CO gas at ppm-level concentration using a single SnO_2 nanowire device. By comparing results before and after functionalization with hybrid Fe-Pd nanocubes, we shed light on the relationship between sensing properties and nanoparticle structure, in particular by characterizing morphological changes induced by sensor operation at elevated temperatures.

SnO_2 nanowires were grown on Si substrates using a synthesis method similar to that previously reported in Reference 19. Chemoresistive sensing devices were constructed on membrane-based TEM heating chips (see ESI), which can be seen in Fig. 1a, with a single SnO_2 nanowire placed across two tungsten (W) contacts as well as across a through-hole for TEM imaging. After electron-beam induced deposition of Pt for improved nanowire-electrode contact properties, both structural and electrical properties were characterized inside the microscope column. The single SnO_2 nanowire exhibited a diameter of 125nm, a length of 15µm between the two W contacts, and was grown along the [100] crystallographic direction, as revealed by high resolution TEM micrographs close to the [010] zone axis (inset of Fig. 1a).

[a] *Nanoparticles by Design Unit, Okinawa Institute of Science and Technology (OIST) Graduate University, 1919-1 Tancha, Onna-Son, Okinawa, 904-0495, Japan. E-mail: mukhles@oist.jp*
[b] *Materials Center Leoben Forschung GmbH, 8700 Leoben, Austria.*

Electronic Supplementary Information (ESI) available: Detailed experimental methods, TEM characterization, additional electrical measurements and results of *ex situ* control experiment. See DOI: 10.1039/x0xx00000x

Nanoscale

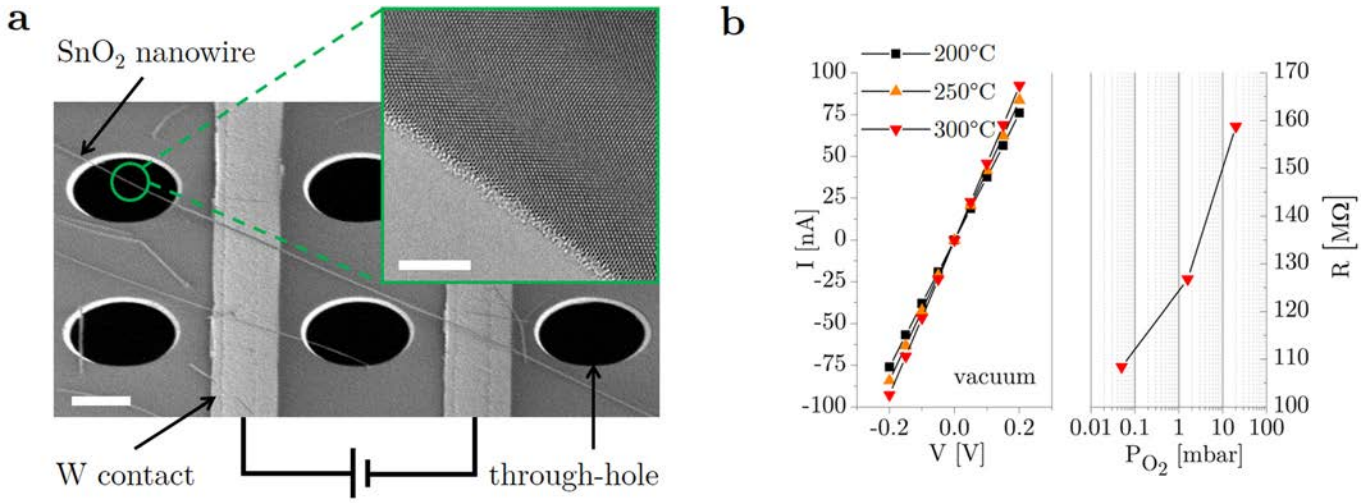

Fig. 1. a) Single SnO_2 nanowire (diameter 125nm) between two W contacts on membrane-based TEM heating chip after mechanical transfer (scale bar 5µm). On the right, a high resolution TEM image close to the [010] zone axis can be seen, revealing the [100] nanowire growth direction (scale bar 5nm). b) *In situ* electrical measurements of the single SnO_2 nanowire in the environmental TEM, showing linear IV characteristics in vacuum at different temperatures (left) and increasing device resistance for increasing O_2 pressures at 300°C (right).

In situ electrical measurements in vacuum showed linear IV characteristics and a weak negative temperature coefficient of nanowire resistance (Fig. 1b, left). Considering the nanowire dimensions and assuming circular geometry, conductivity values of around 5S/cm and a conductivity increase close to 20% at 300°C compared to 200°C were found. Both results are in good agreement with literature results on a single SnO_2 nanowire in N_2 atmosphere.[20] Furthermore, it was found that the device properties were dependent on O_2 gas pressure, with increasing SnO_2 nanowire resistance for increasing O_2 pressure (Fig. 1b, right). This result can be attributed to depletion of electrons close to the surface because of negatively charged ionosorbed oxygen species.[21] Moreover, it is expected that the SnO_2 nanowire initially exhibited a large number of surface oxygen vacancies due to the high-temperature synthesis in oxygen-deficient Ar atmosphere. We assume that a considerable number of these vacancies were compensated upon first exposure to O_2 atmosphere at elevated temperatures, resulting in significantly increased device resistance. Consequently, the single SnO_2 nanowire device clearly shows chemoresistive properties influenced by the gaseous atmosphere in the environmental TEM, confirming the *in situ* functionality.

Nanoparticle decoration is a commonly used method for surface functionalization of nanowire sensor devices in order to optimize chemoresistive properties. In recent years, magnetron sputtering inert-gas condensation has attracted considerable attention for the gas-phase synthesis of nanoparticles with tuneable size, chemical composition and morphology.[22-25] Recently, it was demonstrated that this technique is ideally suited for the single-step decoration of metal oxide nanowire sensor devices with heterogeneous nanocatalysts.[26] In this communication we present bi-metallic Fe-Pd nanoparticles with anisotropic shapes as an exemplary case. A schematic illustration of nanowire decoration by magnetron sputtering inert-gas condensation is shown in Fig. 2. Three individual sputter sources were operated using two Fe targets and one Pd target (see ESI for detailed experimental parameters). The resulting vaporized atomic species were cooled by collisions with Ar gas atoms, resulting in cluster formation.[27] For optimized deposition conditions, Fe-Pd nanoparticles with predominant cuboid morphology (83%) and a narrow size distribution around 9nm were achieved.

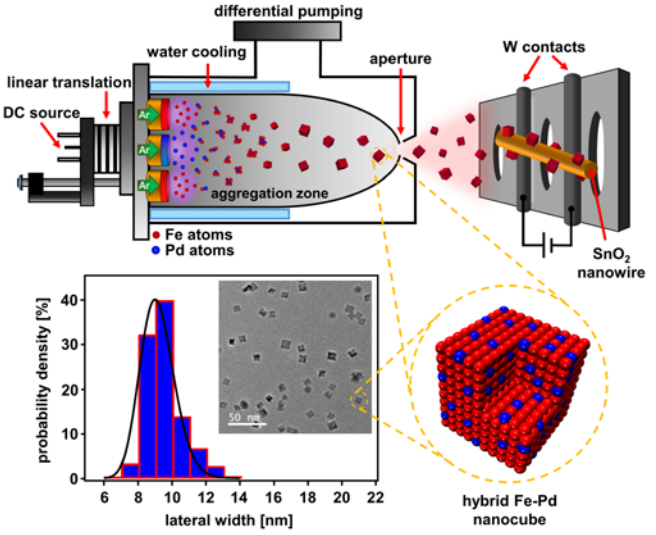

Fig. 2. Schematic illustration of magnetron sputtering-based nanoparticle deposition for surface functionalization of SnO_2 nanowire device with hybrid Fe-Pd nanocubes, exhibiting a narrow size distribution around 9nm (bottom left).

Most commonly, specific nanoparticle shapes are explained by theoretical models based on thermodynamic or kinetic considerations.[28] The mechanism of Fe nanoparticle formation during magnetron sputtering inert-gas condensation has been recently explained by correlating experiments and atomistic modeling.[29] Cubic shapes were found for a certain range of condensation temperatures and atomic deposition rates, clearly underlining the crucial importance of kinetic effects. In a similar way, gas-phase synthesis of hybrid Fe-Pd nanocubes presented in this study is assumed to be governed by an analogous growth mechanism.

Structural characterization of the Fe-Pd nanocubes was performed by high resolution TEM and Fast Fourier Transform (FFT) analysis, which is shown for a representative nanoparticle in Fig. 3. The nanocube core exhibited single-crystalline, body-centred cubic structure with lattice parameters close to Fe. A thin oxide shell was observed on the nanoparticle surfaces, which is attributed to oxidation during ambient air exposure. An epitaxial relationship between this oxide shell and the nanocube core was found. FFT analysis revealed Fe [100] parallel to Fe oxide [100] and Fe [001] parallel to Fe oxide [$0\bar{1}1$], which is in agreement with Reference 30. The lattice spacings corresponding to the shell agree with the inverse-spinel structure characteristic for Fe_3O_4 and Fe_2O_3. Additional scanning TEM micrographs are provided in the ESI (Fig. S1), showing marked contrast differences between metallic core and oxide shell.

Furthermore, electron energy loss spectroscopy (EELS) was employed for compositional characterization. EELS spectra for Fe-Pd nanocube core and shell are compared in Fig. S1. As the nanoparticles were supported on SiN TEM grids, a N-K peak was found in all measurements. The bi-metallic nature of the nanocube core was confirmed, as energy losses for both Pd-$M_{4,5}$ and Fe-$L_{2,3}$ edges were observed. Standard EELS quantification techniques indicate a Pd/Fe ratio of about 5-15% for the core region. In the nanocube shell, no significant amount of Pd was detected. Moreover, the near-edge fine structure of the O-K edge was found to be in good agreement with Fe_3O_4 or Fe_2O_3 and rather different from FeO,[31] which corroborates the results for the Fe-Pd nanocube shell obtained by high resolution TEM.

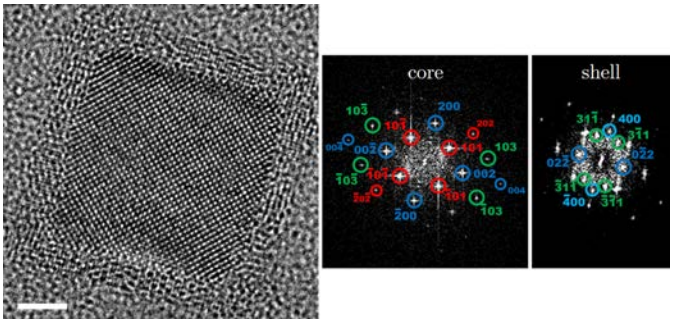

Fig. 3. Characterization of Fe-Pd nanocubes by high resolution TEM imaging and Fast Fourier Transform (FFT) analysis revealed the single-crystalline, body-centred cubic structure of the core, covered by an Fe oxide shell (scale bar 2nm).

The chemoresistive properties of a single SnO_2 nanowire decorated with Fe-Pd nanocubes were studied in the environmental TEM by performing *in situ* carbon monoxide (CO) sensing experiments. The impact of surface functionalization with Fe-Pd nanocubes was assessed by comparing results of the same SnO_2 nanowire before and after nanoparticle deposition. No TEM imaging was performed during CO sensing experiments in order to avoid any potential interference of electron irradiation with the chemoresistive measurements, such as electron beam-induced O_2 gas ionization.

During device operation at 250°C and 20mbar O_2 pressure, a considerable resistance decrease was observed after gradually switching the gas supply from O_2 to 100ppm CO diluted in O_2 (Fig. 4a and Fig. S2), which confirms that CO detection was achieved inside the microscope column. After decoration with Fe-Pd nanocubes, enhanced CO sensor response (39.0±0.5% compared to 33.6±2.3%) and increased device resistance were found, which clearly validates the effect of surface functionalization. No marked structural modifications of the SnO_2 nanowire were observed, either after sensor operation of the pristine SnO_2 nanowire or after measurements subsequent to nanoparticle decoration. Consequently, the differences in sensing properties can be attributed to the influence of Fe-Pd nanoparticles with specific

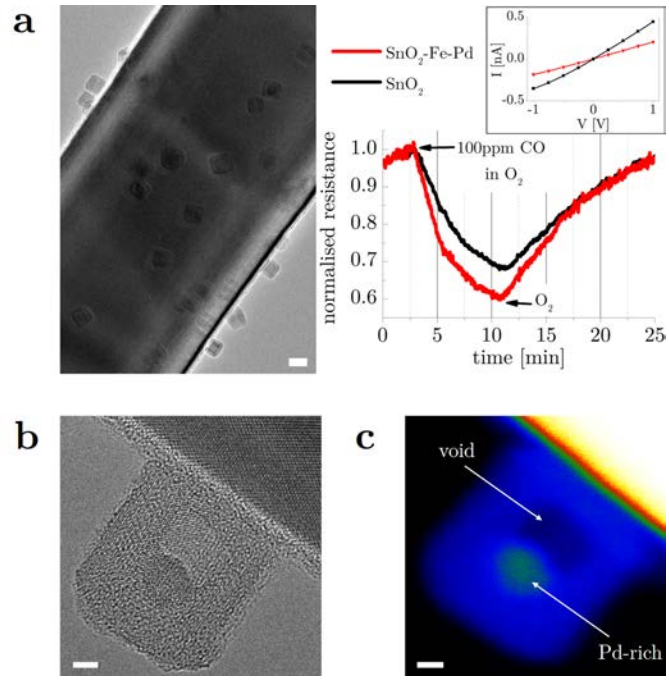

Fig. 4. a) *In situ* chemoresistive sensing of 100ppm CO using a single SnO_2 nanowire functionalized with Fe-Pd nanocubes (scale bar 10nm), compared to measurements before nanoparticle deposition. Electrical measurements were performed at 20mbar O_2 pressure and an operation temperature of 250°C using the same SnO_2 nanowire device. b) Representative Fe-Pd nanoparticle after sensor operation exhibiting considerable structural changes (scale bar 2nm). c) Scanning TEM micrograph of the same Fe-Pd nanocube for visualizing the formation of a void and a Pd-rich region (false color image; scale bar 2nm).

nanoscale structures. Fe-Pd nanoparticles retained cubic shapes but underwent significant morphological changes, in particular void formation combined with the emergence of Pd-rich regions (Fig. 4b, Fig. 4c and Fig. S3).

The presented case of bi-metallic Fe-Pd nanocubes clearly illustrates that information on nanoparticle structure is crucial for the interpretation of sensor performance, for instance in terms of response kinetics or sensitivity. Based on the observed Fe-Pd nanoparticle morphologies, we deduce that changes in SnO_2 nanowire resistance and CO sensing response result from Fe oxide – SnO_2 heterojunctions. Pd was encapsulated in the core and thus not directly influencing the nanowire interface or interacting with the surrounding gas atmosphere. The Fe oxide – SnO_2 interfaces lead to increased electron depletion regions at the nanowire surface in oxygen atmosphere and a more efficient modulation of the conductive nanowire channel in the presence of small concentrations of analyte gases.[32] On the other hand, Pd is not expected to contribute to chemical or electronic sensitization of the SnO_2 nanowire surface, but the Pd-rich core could potentially have an indirect effect by modifying the electronic structure of the Fe oxide shell.

In order to confirm these structural changes, *ex situ* control experiments were performed. After heating Fe-Pd nanocubes to 250°C in ambient air, nanoparticle morphologies similar to those in the *in situ* experiment were observed (see ESI Fig. S4). Consequently, the Pd-rich core/void/shell structure is linked to the specific thermal oxidation behaviour of Fe-Pd nanocubes, which emphasizes the importance of oxidizing reactions during sensor operation in O_2-containing atmospheres. The mechanism giving rise to these morphologies is attributed to the Kirkendall effect with Fe outward diffusion being faster than oxygen inward diffusion.[33] At the same time, Pd stays encapsulated within the Fe oxide shell, comparable to previous reports on Au/Fe oxide core/hollow-shell[34] or other yolk/shell-type nanoparticles.[35]

Hence, our *in situ* TEM approach opens new possibilities for studying nanoparticle morphological changes induced by sensor operation in order to unveil fundamental conductometric sensing mechanisms. It can be applied to elucidate and optimize the sensing performance of chemoresistive devices based on various nanowire-nanoparticle material combinations, which is relevant, for instance, in biomimetic electronic nose systems.[3] Although single-crystalline samples and polycrystalline materials typically show considerable differences in sensing activity,[36] nanowire devices may serve as model systems for other device architectures, providing one-dimensional geometries with well-defined structures. In the future, the presented technique can be used for systematic studies on the morphology dependence of sensing activity and may be combined with *in situ* EELS characterization[37] or light illumination.[38]

Conclusions

In summary, we demonstrate *in situ* chemoresistive sensing in the environmental TEM, studying single SnO_2 nanowire devices functionalized with Fe-Pd nanocubes as exemplary case. We achieve detection of toxic CO gas at ppm-level concentration inside the microscope column, which offers unprecedented opportunities for characterizing structural changes of individual nanoparticles induced by device operation at elevated temperatures. Our novel approach provides information on the nanoscale morphology of heterogeneous nanocatalysts and thus facilitates the interpretation of their influence on sensor performance, offering new opportunities for future optimizations of chemoresistor device technology.

Acknowledgements

This work was supported by funding from OIST Graduate University and has been partly performed within the project "MSP—Multi Sensor Platform for Smart Building Management" (FP7-ICT-2013-10 Collaborative Project, No. 611887).

Notes and references

1 A. Gurlo, *Nanoscale*, 2011, **3**, 154.
2 M. E. Franke, T. J. Koplin, U. Simon, *Small*, 2006, **2**, 36.
3 J. M. Baik, M. Zielke, M. H. Kim, K. L. Turner, A. M. Wodtke, M. Moskovits, *ACS Nano*, 2010, **4**, 3117.
4 B. Liu, D. Cai, Y. Liu, H. Li, C. Weng, G. Zeng, Q. Li, T. Wang, *Nanoscale*, 2013, **5**, 2505.
5 X. Liu, N. Chen, B. Han, X. Xiao, G. Chen, I. Djerdj, Y. Wang, *Nanoscale*, 2015, **7**, 14872.
6 J. Zhang, X. Liu, G. Neri, N. Pinna, *Adv. Mater.*, 2016, **28**, 795.
7 J. Wu, H. Shan, W. Chen, X. Gu, P. Tao, C. Song, W. Shang, T. Deng, *Adv. Mater.*, 2016, **28**, 9686.
8 T. C. Narayan, A. Baldi, A. L. Koh, R. Sinclair, J. A. Dionne, *Nat. Mater.*, 2016, **15**, 768.
9 S. B. Vendelbo, C. F. Elkjær, H. Falsig, I. Puspitasari, P. Dona, L. Mele, B. Morana, B. J. Nelissen, R. van Rijn, J. F. Creemer, P. J. Kooyman, S. Helveg, *Nat. Mater.*, 2014, **13**, 884.
10 J. Wang, Z. Zheng, C. R. Weinberger, Z. Zhang, T. Zhu, S. X. Mao, *Nat. Mater.*, 2015, **14**, 594.
11 D. Jacobsson, F. Panciera, J. Tersoff, M. C. Reuter, S. Lehmann, S. Hofmann, K. A. Dick, F. M. Ross, *Nature*, 2016, **531**, 317.
12 S. Rackauskas, H. Jiang, J. B. Wagner, S. D. Shandakov, T. W. Hansen, E. I. Kauppinen, A. G. Nasibulin, *Nano Lett.*, 2014, **14**, 5810.
13 J. Y. Huang, L. Zhong, C. M. Wang, J. P. Sullivan, W. Xu, L. Q. Zhang, S. X. Mao, N. S. Hudak, X. H. Liu, A. Subramanian, H. Fan, L. Qi, A. Kushima, J. Li, *Science*, 2010, **330**, 1515.
14 M. T. McDowell, I. Ryu, S. W. Lee, C. Wang, W. D. Nix, Y. Cui, *Adv. Mater.*, 2012, **24**, 6034.
15 J. A. Rodríguez-Manzo, Z. J. Qi, A. Crook, J.-H. Ahn, A. T. C. Johnson, M. Drndić, *ACS Nano*, 2016, **10**, 4004.
16 Z. Fan, X. Fan, A. Li, L. Dong, *Nanoscale*, 2013, **5**, 12310.
17 J. Norpoth, S. Mildner, M. Scherff, J. Hoffmann, C. Jooss, *Nanoscale*, 2014, **6**, 9852.
18 L. Li, J. Britson, J. R. Jokisaari, Yi Zhang, C. Adamo, A. Melville, D. G. Schlom, L.-Q. Chen, X. Pan, *Adv. Mater.*, 2016, **28**, 6574.
19 E. Brunet, T. Maier, G. C. Mutinati, S. Steinhauer, A. Köck, C. Gspan, W. Grogger, *Sens. Actuators B*, 2012, **165**, 110.

20 Y. Zhang, A. Kolmakov, S. Chretien, H. Metiu, M. Moskovits, *Nano Lett.*, 2004, **4**, 403.
21 A. Kolmakov, D. O. Klenov, Y. Lilach, S. Stemmer, M. Moskovits, *Nano Lett.*, 2005, **5**, 667.
22 M. Benelmekki, M. Bohra, J.-H. Kim, R. E. Diaz, J. Vernieres, P. Grammatikopoulos, M. Sowwan, *Nanoscale*, 2014, **6**, 3532.
23 V. Singh, C. Cassidy, P. Grammatikopoulos, F. Djurabekova, K. Nordlund, M. Sowwan, *J. Phys. Chem. C*, **118**, 13869.
24 V. Singh, C. Cassidy, F. A. Pedersen, J.-H. Kim, K. Aranishi, S. Kumar, C. Lal, C. Gspan, W. Grogger, M. Sowwan, *Nanoscale*, 2015, **7**, 13387.
25 P. Grammatikopoulos, J. Kioseoglou, A. Galea, J. Vernieres, M. Benelmekki, R. E. Diaz, M. Sowwan, *Nanoscale*, 2016, **8**, 9780.
26 S. Steinhauer, V. Singh, C. Cassidy, C. Gspan, W. Grogger, M. Sowwan, A. Köck, *Nanotechnology*, 2015, **26**, 175502.
27 P. Grammatikopoulos, S. Steinhauer, J. Vernieres, V. Singh, M. Sowwan, *Adv. Phys. X*, 2016, **1**, 81.
28 L. D. Marks, L. Peng, *J. Phys.: Condens. Matter*, 2016, **28**, 053001.
29 J. Zhao, E. Baibuz, J. Vernieres, P. Grammatikopoulos, V. Jansson, M. Nagel, S. Steinhauer, M. Sowwan, A. Kuronen, K. Nordlund, F. Djurabekova, *ACS Nano*, 2016, **10**, 4684.
30 A. Pratt, L. Lari, O. Hovorka, A. Shah, C. Woffinden, S. P. Tear, C. Binns, R. Kröger, *Nat. Mater.*, 2014, **13**, 26.
31 C. Colliex, T. Manoubi, C. Ortiz, *Phys. Rev. B*, 1991, **44**, 11402.
32 K. S. Choi, S. Park, S.-P. Chang, *Sens. Actuators B*, 2017, **238**, 871.
33 H. J. Fan, U. Gösele, M. Zacharias, *Small*, 2007, **3**, 1660.
34 E. V. Shevchenko, M. I. Bodnarchuk, M. V. Kovalenko, D. V. Talapin, R. K. Smith, S. Aloni, W. Heiss, A. P. Alivisatos, *Adv. Mater.*, 2008, **20**, 4323.
35 R. Purbia, S. Paria, *Nanoscale*, 2015, **7**, 19789.
36 A. Gurlo, R. Riedel, *Angew. Chem. Int. Ed.*, 2007, **46**, 3826.
37 J. B. Wagner, P. L. Hansen, A. M. Molenbroek, H. Topsøe, B. S. Clausen, S. Helveg, *J. Phys. Chem. B*, 2003, **107**, 7753.
38 J. B. Wagner, F. Cavalca, C. D. Damsgaard, L. D. L. Duchstein, T. W. Hansen, *Micron*, 2012, **43**, 1169.